J. Beerten and R. Belmans, “A Comprehensive Modeling Framework for Dynamic and Steady-State Analysis of Voltage Droop Control Strategies in HVDC Grids,” *International Journal of Electrical Power & Energy Systems*, vol. 73, pp. 691–701, Dec. 2015.

Digital Objective Identifier: 10.1016/j.ijepes.2015.05.030

URL:
http://www.sciencedirect.com/science/article/pii/S0142061515002355

A Comprehensive Modeling Framework for Dynamic and Steady-State Analysis of Voltage Droop Control Strategies in HVDC Grids

J. Beerten[a,*], R. Belmans[a]

[a] *K.U.Leuven, Division of Electrical Energy and Computer Architectures (ESAT-ELECTA), Kasteelpark Arenberg 10, bus 2445, 3001 Leuven, Belgium*

Abstract

This paper presents a comprehensive modeling framework to analyse and compare the performance of different voltage droop control characteristics in an HVDC grid. All models are fully derived mathematically, both for dynamic simulations and for steady-state power flow analysis. The main contribution lies in the development of a common modeling and control approach for the different droop-based control schemes that have been presented in the literature. The discussion includes power-and current-based droop control, either in their standard form or combined with a deadband, a constant voltage control or consisting of different slopes. Dynamic simulations show that, when applying a comparable underlying dynamic converter control framework, similar dynamic responses can be expected from the different droop control schemes, while the steady-state voltage deviations and power sharing after a contingency are different. A comparison with results from a full-detailed power flow implementation shows that these voltage deviations and power sharing can accurately be predicted by the derived steady-state power flow models, thereby avoiding the need for time-consuming dynamic simulations.

Keywords: HVDC transmission, Power system modeling, Load flow analysis, VSC HVDC.

1. Introduction

Since its introduction in the late 1990s, the power engineering community's interest in Voltage Source Converter High Voltage Direct Current (VSC HVDC) technology has increased significantly. The technology is also the preferred candidate for offshore HVDC grids or an HVDC supergrid [1], due to the good prospects the technology has when it comes to an operation in a multi-terminal (MTDC) set-up. In recent year, the modeling and control of these multi-terminal configurations has gained significant interests in the research community.

Much research has been focusing on the use of a so-called voltage droop control [2, 3], as an alternative to the earlier proposed voltage margin control schemes [4–6]. A voltage droop control is a truly distributed

*Corresponding author. Tel.: +32 16 32 10 20, Fax.: +32 16 32 19 85.
Email addresses: jef.beerten@esat.kuleuven.be (J. Beerten), ronnie.belmans@esat.kuleuven.be (R. Belmans)

control, in the sense that different converters independently contribute to the dc-side voltage control at the same time. In the literature, the voltage droop control has been modeled in different ways. As discussed in [7], a first distinction can be made between power-based [2, 3, 8–11] and current-based [12–15] droop control, depending on whether the droop control is expressed in terms of active power or dc-side current. A power-based droop control seems the most obvious option from an ac grid perspective. However, the current-based variants result in a linear control of the voltage in the network. Alternatively, a deadband can be included in the droop control [8], or the droop control can be combined with a constant voltage control [16]. It is also possible to use a piecewise linear droop characteristic with different gains, as presented in [17]. After the primary response caused by the droop control, a slower secondary control can be implemented to reschedule the power flows between different interconnected systems, as discussed in [18]. Similarly, the controllers can be extended with outer control loops to damp inter-area oscillations [19, 20].

Until recently, most research efforts have been dedicated towards the dynamic control behavior of the voltage droop. And although droop control is primarily intended for a fast coordinated response to share the power deficit caused by a contingency, the droop characteristics also have an important influence on the steady-state power flows [10, 21], since they give rise to a steady-state change of converter power injections. When these droop characteristics are not designed appropriately, the dc-side voltage and power injections deviate from their setpoint values, as studied in [22] or might cause overloading transmission lines [23]. At the same time, the droop control can interact with a frequency droop, as analyzed in [24, 25]. However, little research has been conducted so far to provide a common modeling approach, which allows to compare the response of different droop characteristics and to benchmark the results obtained using power flow models with the steady-state results of dynamic models. Although there is a general consensus on the importance of droop control for future HVDC grids, little effort has been undertaken in general to compare the many distinguishable droop control concepts. In [7], different dc-side voltage control concepts for HVDC grids have been reviewed, but the analysis has been limited to a conceptual discussion without covering the actual control implementation and modeling.

This paper aims to address this lacune by developing a comprehensive modeling framework, both for the dynamic control structure as well as for the steady-state representation, to evaluate the different droop-based control characteristics. The main contribution of this work is the development, the analytical derivation and comparison of a wide variety of voltage-droop characteristics. First, the paper introduces a clear and concise overview of dc-side voltage control and droop control in particular in Section 2. In Section 3, the corresponding analytical models for both a steady-state and dynamic implementation are derived for the different droop control characteristics presented in the literature. The paper is concluded with a practical implementation of these control characteristics in a 4-terminal meshed HVDC grid, using both a transient stability program and a power flow program, and the similarities and differences in dynamic response and steady-state operating conditions after a setpoint change and a converter outage are analyzed.

2. Droop control fundamentals

This section summarizes the main principles of the active power and dc-side voltage control in an HVDC grid and discusses the importance of droop control in this respect. In a second part, the different options for the practical dynamic implementation of the droop control are introduced.

2.1. Converter dc-side voltage and power control principles

In converter control, it is common practice to control the inner VSC current control loops using a rotating dq-reference frame which is locked to the rotating ac system voltage vector by means of a Phase Locked Loop (PLL). As a consequence of this control, the converter current is decoupled into components related to the active and reactive power control. In this article, the q-component is aligned with the ac system voltage u_s. A number of control functions can be distinguished with respect to this current component aligned with the ac-side voltage and thus linked with the active power.

1. P_{ac} *constant*: Constant active power injection into the ac system.
2. P_{dc} *constant*: Constant active power injection into the dc system.
3. I_{dc} *constant*: Constant dc-side current injection into the dc system.
4. U_{dc} *constant*: The current order is changed to control the dc-side voltage U_{dc} to a constant value.
5. U_{dc} *droop*: Dependent on the actual value of the dc-side voltage U_{dc}, the current order is changed.

For the sake of completeness, it should be mentioned that different control options can be defined for the d-component of the converter current, such as constant Q, constant U or a droop-based ac-side voltage control. However, the control of reactive power is out of the scope of this paper and will not be discussed further.

2.2. General droop control definition

Since the control of the dc-side voltage is of utmost importance to the operation of the HVDC grid, there is a consensus in the research on HVDC grids to distribute this control over different converters, preferably by means of a proportional droop control action. Depending on the variable chosen, the droop control law can be defined in different ways:

1. $U_{dc} - P_{ac}$ *droop*: ac-side active power reference P_s^* changes.
2. $U_{dc} - P_{dc}$ *droop*: dc-side power reference P_{dc}^* changes.
3. $U_{dc} - I_{dc}$ *droop*: dc-side current reference I_{dc}^* changes.

with P_s the active power at the Point of Common Coupling (PCC). Using existing control concepts from two-terminal schemes, the $U_{dc}-P_{ac}$ droop option seems the most straightforward option. From a system's point of view, the $U_{dc}-I_{dc}$ droop relation is the one that is directly linked to the voltage dynamics in the dc

system . Alternatively, the droop equation can be based on the active dc-side power ($U_{dc}-P_{dc}$), which only differs from a $U_{dc}-P_{ac}$ droop through the converter losses. However, since it is common practice to neglect the converter losses in the dynamic analysis, as e.g. done in [2, 3, 8–10, 12–14, 26], this simplification has also been used in this paper, implying that a $U_{dc} - P_{ac}$ and $U_{dc} - P_{dc}$ droop give rise to similar results. Alternatively, a first approximation could be to only neglect the change in converter losses between different setpoints, rendering a constant converter los representation for the dynamic analysis.

The principle of a distributed control by means of a droop control can also be combined with a constant power/current control, a constant voltage control or a droop control with another control gain to distinguish between normal and disturbed operation [7]. Fig. 1 shows the possibilities to combine the principles of droop control with different control characteristics around the reference point.

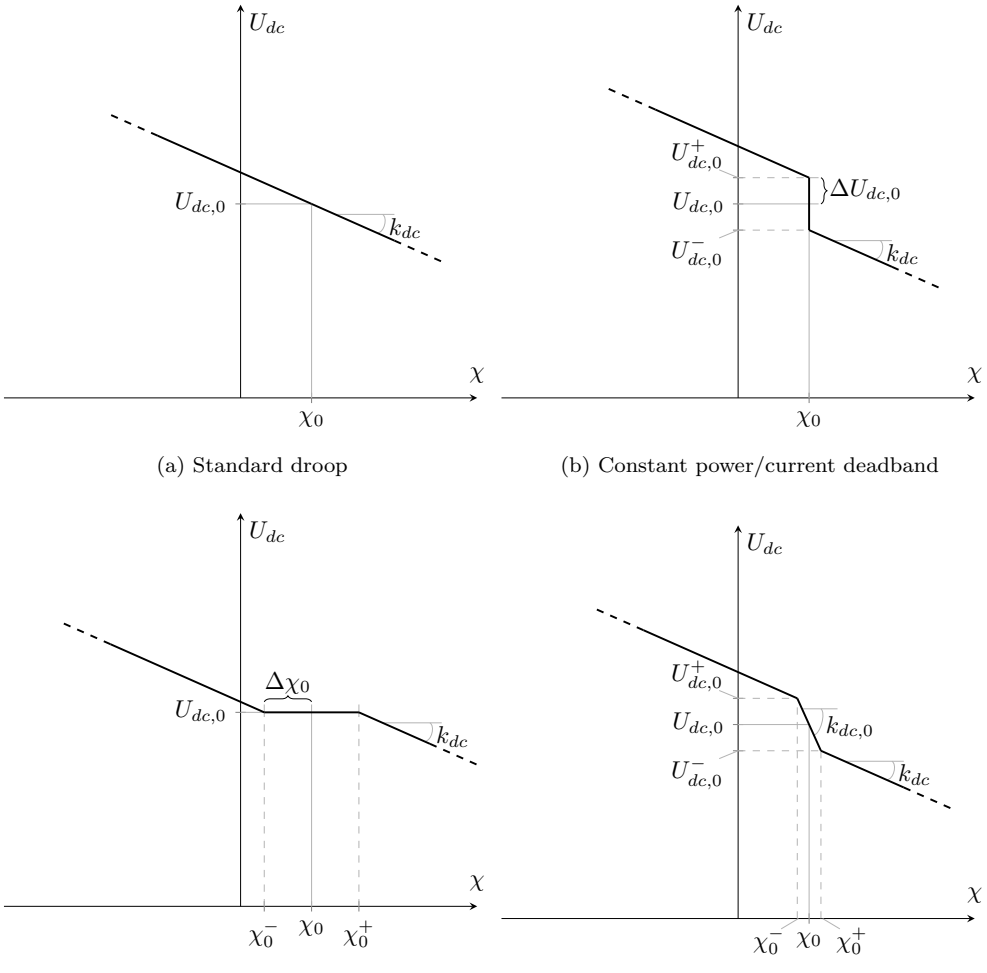

(a) Standard droop

(b) Constant power/current deadband

(c) Constant voltage band

(d) Piecewise linear droop

Figure 1: Converter voltage droop-based control characteristics.

For completeness, a generalized variable χ has been used as a control variable, which can be defined as

$$\chi = \begin{cases} -P_s & \text{ac power-based droop} \\ P_{dc} & \text{dc power-based droop} \\ I_{dc} & \text{dc current-based droop} \end{cases}, \tag{1}$$

Hereby we take the convention that the ac- and dc-side powers and currents are positive when respectively injected into the ac and dc system .

For the sake of completeness, it should be mentioned that in the literature, examples are found of using the square of the dc-side voltage for constant voltage control [27] or for droop control [28]. As an alternative to using a local voltage signal, in [29] it has been suggested to use a common (voltage) feedback signal for all converters instead of the local voltage values, thereby altering the power sharing by using communication.

2.3. Dynamic implementation of droop control

The proportional droop control can be implemented in various ways. In Fig. 2, a generalized implementation has been depicted in which the droop control law (U_{dc} droop) is followed by a conversion block to convert dc-side quantities (for example current I_{dc} or power P_{dc}) to the ac-side current reference $i_{cq}^{'*}$ before limiting.

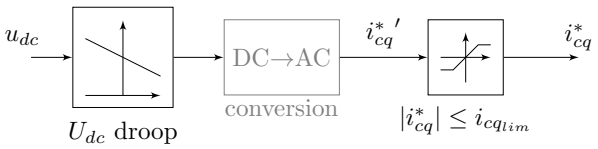

Figure 2: Direct droop control implementation.

In case of an $U_{dc} - P_{ac}$ droop, the conversion block can be omitted and replaced by a division with u_s, the voltage at the PCC. In this control layout, the droop control law is thus directly linked with the inner current controllers, as done in [12, 13, 26]. A disadvantage of the direct droop implementation from Fig. 2 is that the conversion block can cause ac- and dc-side voltage dynamics to enter the controller, making that they can easily propagate through the inner current controller if no precautions are being taken. Alternatively, the droop control can be integrated with an active power control. This is shown in Fig. 3, where a power change ΔP_s is added to the power setpoint $P_{s,0}$. As the analysis in [30] shows, an implementation using a PI power controller is preferred over a feedforward power loop in order to avoid high-gain instability problems. The output of the PI power controller can be directly connected to the inner current reference signal or can be the input signal of a cascaded structure with an internal dc-side voltage PI controller, as recently developed in [31]. A similar control structure has been proposed in [32]. The advantage of cascading an internal dc-side voltage controller in the structure, is that local clamping of the dc-side voltage is still possible, e.g. in the case of an isolation of the converter or when a voltage limit is hit [31]. This makes it a good candidate for an

internal converter control structure to be augmented with different droop characteristics, and in particular for those combining droop control with a constant voltage control (Fig. 1c).

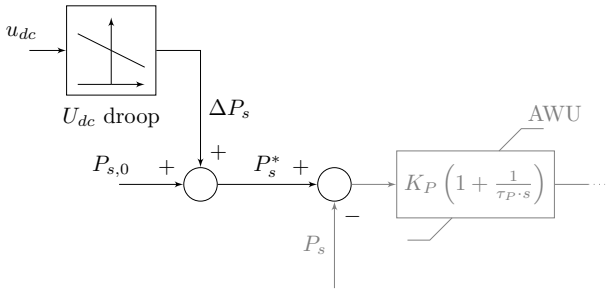

Figure 3: Voltage droop control implementation as a contribution to an outer active power controller.

For these reasons, the analysis of the dynamic implementation in this paper is based on a cascaded control structure where the droop is implemented as an outer control layer. Consequently, all droop control equations need to be reformulated so that they are represented in terms of an active power contribution ΔP_s as a function of the dc-side voltage U_{dc} .

2.4. Steady-state implementation of droop control

Another important consequence of the droop control are the changes in the power flows it causes throughout the entire system after contingencies (converter or line outage) or after setpoint changes. These steady-state effects can be studied by including droop characteristics in the dc system power flow representation. Consequently, the droop control also causes changes in the power flows in the connected ac networks. In this paper, however, the emphasis is on the HVDC grid control and therefore only the dc system power flow is discussed.

In a generalized HVDC grid with n buses, the power flow equations can be written as

$$I_{dc_i} = \sum_{\substack{j=1 \\ j \neq i}}^{n} Y_{dc_{ij}} \cdot (U_{dc_i} - U_{dc_j}), \tag{2}$$

or in terms of active powers

$$P_{dc_i} = p\, U_{dc_i} \sum_{\substack{j=1 \\ j \neq i}}^{n} Y_{dc_{ij}} \cdot (U_{dc_i} - U_{dc_j}). \tag{3}$$

with $Y_{dc_{ij}}$ the dc branch admittances equal to $1/R_{dc_{ij}}$ and $p = 1$ for a monopolar system or $p = 2$ for a monopolar symmetrically grounded or bipolar system. This system of equations can be solved by a Newton-Raphson method

$$\left(\boldsymbol{U_{dc}} \frac{\partial \boldsymbol{P_{dc}}}{\partial \boldsymbol{U_{dc}}}\right)^{(j)} \cdot \frac{\boldsymbol{\Delta U_{dc}}^{(j)}}{\boldsymbol{U_{dc}}} = \boldsymbol{\Delta P_{dc}}^{(j)}. \tag{4}$$

However, in case of a droop control at a particular bus, the active power injection at that bus is not known in advance and depends on the actual value of the dc-side voltage at the bus, which is the variable solved for in (4). This problem can be circumvented by modifying the vector with active power injections $\boldsymbol{P_{dc}}$ from (4) and reformulating the problem [33] such that

$$\left(\boldsymbol{U_{dc}}\frac{\partial \boldsymbol{X_{dc}}}{\partial \boldsymbol{U_{dc}}}\right)^{(j)} \cdot \frac{\boldsymbol{\Delta U_{dc}}^{(j)}}{\boldsymbol{U_{dc}}} = \boldsymbol{\Delta X_{dc}}^{(j)}, \tag{5}$$

with $\boldsymbol{X_{dc}}$ a generalized vector, including droop setpoints instead of the yet unknown active power injections.

In the next section, the representation of the different droop characteristics in this active power-based representation of the power flow algorithm are discussed.

3. Droop control representation

This section discusses the representation and implementation of the droop control, both for dynamic system studies, as well as for power flow studies. The section thus aims at deriving the mathematical representation for the different droop representations from Fig. 1, both for power- and current-based droop control.

3.1. Standard droop control

The general droop control law as depicted in Fig. 1a is defined as

$$\chi = \chi_0 - \frac{1}{k_{dc}}(U_{dc} - U_{dc,0}), \tag{6}$$

with χ a generalized flow variable as defined in (1) that can either represent the power or current. In case of a power-based droop control, the control law is defined as

$$P_{dc} = P_{dc,0} - \frac{1}{k_{dc}}(U_{dc} - U_{dc,0}), \tag{7}$$

whereas in the case of a current-based droop control, the droop equation is rewritten as

$$I_{dc} = I_{dc,0} - \frac{1}{k_{dc}}(U_{dc} - U_{dc,0}). \tag{8}$$

3.1.1. Dynamic representation

The power-based droop is the most straightforward way of implementing a droop control from a dynamic point of view. Replacing P_{dc} and $P_{dc,0}$ from (7) with respectively $-P_s$ and $-P_{s,0}$, the negative of the ac-side active power setpoint and its reference, the equation can be rewritten in terms of an incremental power contribution $\Delta P_s = P_s - P_{s,0}$

$$\Delta P_s = \frac{1}{k_{dc}}(U_{dc} - U_{dc,0}). \tag{9}$$

This control law can directly be included in the control structure from Fig. 3.

It is equally possible to implement the current-based droop control dynamically by means of a an outer control layer (Fig. 3), which requires rewriting the droop characteristics in terms of an active power deviation ΔP_{dc}. Hence, considering the intersection $U_{dc,I0}$ of the droop characteristic with the U_{dc}-axis in Fig. 1a, the current-based droop equation (8) can be rewritten as

$$I_{dc}{=}-\frac{1}{k_{dc}}(U_{dc}-U_{dc,I0}), \tag{10}$$

with

$$U_{dc,I0}{=}U_{dc,0}+k_{dc}I_{dc,0}. \tag{11}$$

With the active dc-side power P_{dc} defined as

$$P_{dc}=pU_{dc}I_{dc}, \tag{12}$$

the active power deviation ΔP_{dc} is rewritten as

$$\Delta P_{dc}{=}P_{dc}-P_{dc,0}, \tag{13}$$

$$=p\left(U_{dc}I_{dc}-U_{dc,0}I_{dc,0}\right). \tag{14}$$

Substituting $I_{dc,0}$ for I_{dc} in (10) and substituting the obtained expression for $I_{dc,0}$ in (14) together with I_{dc} from (10), ΔP_{dc} becomes

$$\Delta P_{dc}=-\frac{p}{k_{dc}}\left[\left(U_{dc}^2-U_{dc,0}^2\right)-U_{dc,I0}\left(U_{dc}-U_{dc,0}\right)\right]. \tag{15}$$

When neglecting the converter losses for the dynamic analysis, the negative of (15) yields an expression for ΔP_s in terms of U_{dc}, which can directly be integrated into the control structure from Fig. 3.

3.1.2. Steady-state representation

Whereas the dc-side powers of the constant power controlled buses are known prior to a dc system power flow, this is not the case for droop controlled buses. For a power-based droop control at bus i, X_{dc_i} from (5) can be defined equal to the power setpoint of the droop control $P_{dc,0}$. Hence, rewriting (7)

$$X_{dc_i}=P_{dc,0_i}=P_{dc_i}+\frac{1}{k_{dc_i}}(U_{dc_i}-U_{dc,0_i}), \tag{16}$$

the corresponding mismatch $\Delta X_{dc_i}^{(j)}$, the i-th element in the mismatch vector for the j-th iteration $\boldsymbol{\Delta X_{dc}}^{(j)}$ from (5) is given by

$$\Delta X_{dc_i}^{\prime(j)}{=}P_{dc,0_i}-P_{dc,0_i}(\boldsymbol{U_{dc}}^{(j)}), \tag{17}$$

with $P_{dc,0_i}(\boldsymbol{U_{dc}}^{(j)})$ as

$$P_{dc,0_i}^{(j)}=P_{dc_i}(\boldsymbol{U_{dc}}^{(j)})+\frac{1}{k_{dc_i}}(U_{dc_i}^{(j)}-U_{dc,0_i}) \tag{18}$$

and with $P_{dc_i}(\boldsymbol{U_{dc}}^{(j)})$ given by (3) evaluated for $\boldsymbol{U_{dc}}^{(j)}$. The corresponding Jacobian terms change to

$$\left(U_{dc_j}\frac{\partial P_{dc,0_i}}{\partial U_{dc_j}}\right)^{(j)} = \left(U_{dc_j}\frac{\partial P_{dc_i}}{\partial U_{dc_j}}\right)^{(j)} = -pU_{dc_i}^{(j)}Y_{dc_{ij}}U_{dc_j}^{(j)}, \tag{19}$$

$$\left(U_{dc_i}\frac{\partial P_{dc,0_i}}{\partial U_{dc_i}}\right)^{(j)} = \left(U_{dc_i}\frac{\partial P_{dc_i}}{\partial U_{dc_i}}\right)^{(j)} + k_{dc_i}^{-1}U_{dc,i}^{(j)}, \tag{20}$$

meaning that only the diagonal elements for the buses with droop control need to be altered.

Similarly, in the case of a current-based droop control, (8) is rewritten such that

$$X_{dc_i} = I_{dc,0_i} = I_{dc_i} + \frac{1}{k_{dc_i}}(U_{dc_i} - U_{dc,0_i}), \tag{21}$$

so that the mismatch $\Delta X_{dc_i}^{(j)}$ is given by

$$\Delta X_{dc_i}^{(j)} = I_{dc,0_i} - I_{dc,0_i}(\boldsymbol{U_{dc}}^{(j)}), \tag{22}$$

with $I_{dc,0_i}(\boldsymbol{U_{dc}}^{(j)})$ as

$$I_{dc,0_i}^{(j)} = I_{dc_i}(\boldsymbol{U_{dc}}^{(j)}) + \frac{1}{k_{dc_i}}(U_{dc_i}^{(j)} - U_{dc,0_i}) \tag{23}$$

and with $I_{dc_i}(\boldsymbol{U_{dc}}^{(j)})$ given by (2) evaluated for $\boldsymbol{U_{dc}}^{(j)}$. The modified Jacobian elements are thus given by

$$\left(U_{dc_j}\frac{\partial I_{dc,0_i}}{\partial U_{dc_j}}\right)^{(j)} = -U_{dc_j}^{(j)}Y_{dc_{ij}}, \tag{24}$$

$$\left(U_{dc_i}\frac{\partial I_{dc,0_i}}{\partial U_{dc_i}}\right)^{(j)} = U_{dc_i}^{(j)}\sum_{\substack{j=1\\ j\neq i}}^{n} Y_{dc_{ij}} + k_{dc_i}^{-1}U_{dc,i}^{(j)}. \tag{25}$$

Hence, also the non-diagonal elements of row i change because of the current-based character of the droop.

3.2. Deadband droop control

Alternatively, a deadband can be included by rewriting the droop characteristics such that

$$\chi = \chi_0 - \frac{1}{k_{dc}}(U_{dc} - U'_{dc,0}), \tag{26}$$

with

$$U'_{dc,0} = \begin{cases} U_{dc,0}^{-} & \text{if } U_{dc} \leq U_{dc,0}^{-} \\ U_{dc} & \text{if } U_{dc,0}^{-} < U_{dc} < U_{dc,0}^{+} \\ U_{dc,0}^{+} & \text{if } U_{dc,0}^{+} \leq U_{dc} \end{cases}, \tag{27}$$

with $U_{dc,0}^{-} = U_{dc,0} - \Delta U_{dc,0}$ and $U_{dc,0}^{+} = U_{dc,0} + \Delta U_{dc,0}$ and $\Delta U_{dc,0}$ the width of half of the deadband as in Fig. 1b. Similar to (6), χ and χ_0 can be replaced with their corresponding variables for dc-side power or dc-side current, resulting in the expressions for a power-or current-based droop control with deadband.

3.2.1. Dynamic representation

The dynamic representation of the power-based deadband droop control is similar to that of a standard droop control, namely

$$\Delta P_s = \frac{1}{k_{dc}}(U_{dc} - U'_{dc,0}), \tag{28}$$

with $U'_{dc,0}$ defined as defined in (27). Hence, the active power contribution ΔP_s will be different from zero when the voltage moves outside of the deadband.

In case of a current-based droop control with a constant current deadband, ΔP_{dc} from (15) can be reformulated as

$$\Delta P_{dc} = \Delta P_{dc_\alpha} + \Delta P_{dc_\beta}, \tag{29}$$

with the two contributing terms ΔP_{dc_α} and ΔP_{dc_β} given by

$$\Delta P_{dc_\alpha} = -\frac{p}{k_{dc}} \left[\left(U_{dc}^2 - U_{dc,0}'^2 \right) - U'_{dc,I0} \left(U_{dc} - U'_{dc,0} \right) \right], \tag{30}$$

$$\Delta P_{dc_\beta} = p I_{dc,0} (U'_{dc,0} - U_{dc,0}), \tag{31}$$

with $U'_{dc,0}$ as defined in (27) and $U'_{dc,I0}$ defined as

$$U'_{dc,I0} = U'_{dc,0} + k_{dc} I_{dc,0}. \tag{32}$$

As shown in Fig. 4a, the first term ΔP_{dc_α} stems from the actual droop implementation and is zero when the current is constant. The second term ΔP_{dc_β} corrects for the deadband and the resulting power variation under constant current control due to the change in dc-side voltage. The quadratic dependence from (30) is not apparent from this graph and it can be shown that a very high droop factor k_{dc} is needed to visualize it.

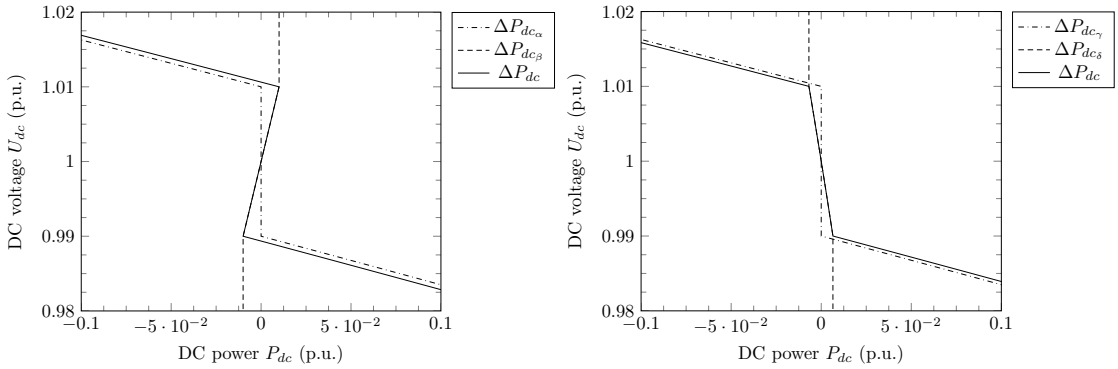

(a) Deadband droop control

(b) Piecewise linear droop control

Figure 4: Current-based droop control – active power contributions.

3.2.2. Steady-state representation

The inclusion of the deadband in the power-based droop control results in a redefinition of $P_{dc,0_i}$ in (17), namely

$$P_{dc,0_i}^{(j)} = P_{dc_i}(\boldsymbol{U_{dc}}^{(j)}) + \frac{1}{k_{dc_i}}(U_{dc_i}^{(j)} - U'_{dc,0_i}), \tag{33}$$

with $U'_{dc,0_i}$ at bus i as defined in (27). Consequently, this leads to a redefinition of the diagonal Jacobian term (20)

$$\left(U_{dc_i}\frac{\partial P_{dc,0_i}}{\partial U_{dc_i}}\right)^{(j)} = \left(U_{dc_i}\frac{\partial P_{dc_i}}{\partial U_{dc_i}}\right)^{(j)} + \alpha_i^{(j)}, \tag{34}$$

with

$$\alpha_i^{(j)} = \begin{cases} k_{dc_i}^{-1}U_{dc,i}^{(j)} & \text{if } U_{dc_i}^{(j)} \neq U'_{dc,0_i} \\ 0 & \text{if } U_{dc_i}^{(j)} = U'_{dc,0_i} \end{cases}. \tag{35}$$

whereas for the non-diagonal elements, (19) remains valid. This means that, when the dc-side voltage is within the deadband, the representation becomes equal to that of a constant power converter.

In the case of a current-based droop control, similarly $I_{dc,0_i}(\boldsymbol{U_{dc}}^{(j)})$ is rewritten using $U'_{dc,0}$ as

$$I_{dc,0_i}^{(j)} = I_{dc_i}(\boldsymbol{U_{dc}}^{(j)}) + \frac{1}{k_{dc_i}}(U_{dc_i}^{(j)} - U'_{dc,0_i}), \tag{36}$$

and the diagonal Jacobian term (25) is consequentially redefined as

$$\left(U_{dc_i}\frac{\partial I_{dc,0_i}}{\partial U_{dc_i}}\right)^{(j)} = U_{dc_i}^{(j)}\sum_{\substack{j=1 \\ j\neq i}}^{n} Y_{dc_{ij}} + \alpha_i^{(j)}. \tag{37}$$

with $\alpha_i^{(j)}$ from (35). This means that, when operating in the deadband, the bus is represented by a constant dc-side current injection. The non-diagonal Jacobian elements are still defined by (24).

3.3. Droop control with constant voltage band

The characteristics of a deadband droop control, (26) – (27) from the previous section, can be considered as the combination of a constant power (or current) and droop control characteristics. It is also possible to combine a constant voltage control characteristic with that of a droop control, as shown in Fig. 1c. In this case, the droop characteristics are described by

$$\begin{cases} U_{dc} = U_{dc,0} & \text{if } \chi_0^- < \chi < \chi_0^+ \\ \chi = \chi_0^- - k_{dc}^{-1}(U_{dc} - U_{dc,0}) & \text{if } \chi \leq \chi_0^- \\ \chi = \chi_0^+ - k_{dc}^{-1}(U_{dc} - U_{dc,0}) & \text{if } \chi_0^+ \leq \chi \end{cases}. \tag{38}$$

Similar to the previous cases, χ can either represent the active power P_{dc} or current I_{dc}.

3.3.1. Dynamic representation

Although the characteristics combining a deadband (Fig. 1b) or a constant voltage band (Fig. 1c) with a standard droop control might appear to be similar, there is a fundamental difference: whereas the deadband results in the absence of a voltage-dependent control action for small voltage deviations from the reference value, the constant voltage band implies a control action forcing these voltage deviation to zero by changing the power. This means that an active control of the dc-side voltage, e.g. based on a PI control action, has to be included.

The voltage control law from (38) can be implemented using a cascaded control structure as shown in Fig. 5. The cascaded control layout is based on the design proposed in [31] and has been altered to include a

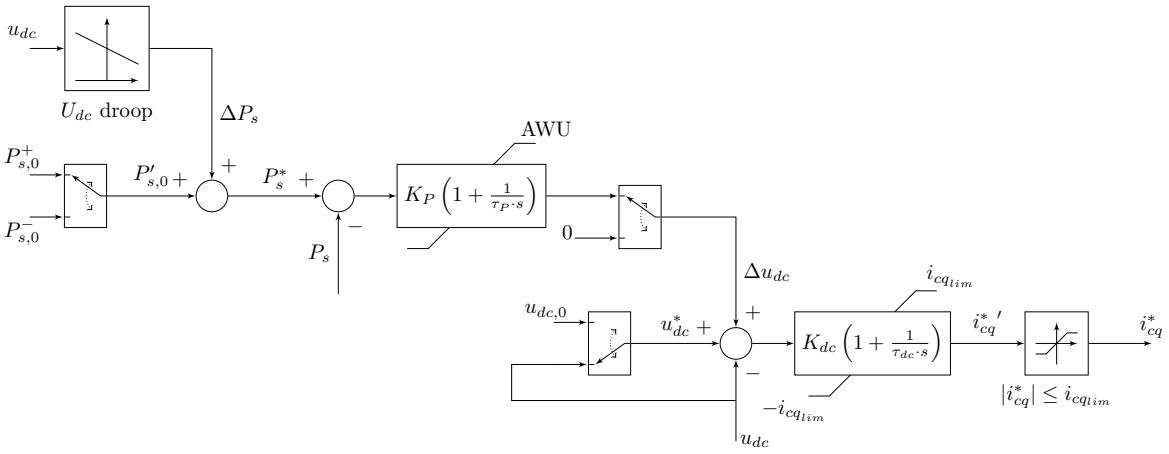

Figure 5: Dynamic implementation of droop control with constant voltage band.

constant voltage band to the droop control. The active power controller with droop control from Fig. 3 has been cascaded with an inner PI controller, which allows the dc-side voltage to be controlled to its reference value.

The constant voltage control law is given by

$$U^*_{dc}=\begin{cases} U_{dc,0} & \text{if } |i^*_{cq}-i_{cq,0}|<\Delta i_{cq,0} \\ U_{dc} & \text{if } |i^*_{cq}-i_{cq,0}|\geq \Delta i_{cq,0} \end{cases}, \tag{39}$$

with $i_{cq,0} = P_{s,0}/u_{sq}$ and $\Delta i_{cq,0} = \Delta P_{s,0}/u_{sq}$ and u_{sq} the system voltage. This means that the dc-side voltage control is only active when the control efforts are within the limits dictated by $P^-_{s,0}$ and $P^+_{s,0}$. The active power controller is only active when the controller operates outside of the constant voltage region, by letting

$$P'_{s,0}=\begin{cases} P^-_{s,0} & \text{if } i^*_{cq}-i_{cq,0}\leq -\Delta i_{cq,0} \\ P^+_{s,0} & \text{if } i^*_{cq}-i_{cq,0}\geq \Delta i_{cq,0} \end{cases}. \tag{40}$$

When the dc-side voltage control is active, the active power contribution in the voltage reference Δu_{dc} is put equal to zero and the anti-windup (AWU) of the PI power controller is activated.

In case of a power-based control, ΔP_s can be taken directly from (9). In case of a current-based control, the current values $I^-_{dc,0}$ and $I^+_{dc,0}$ can be written in terms of active power

$$P^-_{dc,0}{=}p\, U_{dc,0} I^-_{dc,0}, \tag{41}$$

$$P^+_{dc,0}{=}p\, U_{dc,0} I^+_{dc,0}. \tag{42}$$

The active power deviation corresponding to the voltage deviation can be derived from (15)

$$\Delta P_{dc} = -\frac{p}{k_{dc}} \left[\left(U^2_{dc} - U^2_{dc,0}\right) - U''_{dc,I0} \left(U_{dc} - U_{dc,0}\right) \right], \tag{43}$$

with now a different expression for the intersection of the droop characteristics with the U_{dc}-axis in Fig. 1c

$$U''_{dc,I0}{=}U_{dc,0} + k_{dc} I'_{dc,0}, \tag{44}$$

and $I'_{dc,0}$ respectively $I^-_{dc,0}$ and $I^+_{dc,0}$ for the two droop controlled regions. Assuming a lossless converter, $P^-_{s,0}$, $P^+_{s,0}$ and ΔP_s are given by the negative of the values from (41) – (43).

3.3.2. Steady-state representation

The combination of a droop control and a constant voltage control can be implemented by adding an outer loop to the dc system power flow. The respective bus is either initiated as a droop controlled bus or a constant voltage bus and can change during the iteration.

In case of a power-based droop control, the active power setpoint $P_{dc,0_i}$ and $P_{dc,0_i}(\boldsymbol{U_{dc}}^{(j)})$, its evaluation at $\boldsymbol{U_{dc}}^{(j)}$ in (17), both need to be replaced with the following expressions

$$P^-_{dc,0}{=}\, P_{dc} + k^{-1}_{dc}(U_{dc} - U_{dc,0}) \text{ if } \; P_{dc} \leq P^-_{dc,0}, \tag{45}$$

$$P^+_{dc,0}{=}\, P_{dc} + k^{-1}_{dc}(U_{dc} - U_{dc,0}) \text{ if } \; P_{dc} \geq P^+_{dc,0}. \tag{46}$$

When, as a result of the dc system power flow, the active power deviation $|P_{dc} - P_{dc,0}|$ becomes smaller than $\Delta P_{dc,0}$, the respective node is set to a constant voltage node and the power flow calculation is repeated until no change in operation regime is detected between two subsequent iteration cycles.

Similarly, in case of a constant current droop, the current setpoint $I_{dc,0}$ and $I_{dc,0_i}(\boldsymbol{U_{dc}}^{(j)})$ in (22) are replaced with either

$$I^-_{dc,0}{=}\, I_{dc} + k^{-1}_{dc}(U_{dc} - U_{dc,0}) \text{ if } \; I_{dc} \leq I^-_{dc,0}, \tag{47}$$

$$I^+_{dc,0}{=}\, I_{dc} + k^{-1}_{dc}(U_{dc} - U_{dc,0}) \text{ if } \; I_{dc} \geq I^+_{dc,0}, \tag{48}$$

depending on the value of I_{dc}. The other equations remain valid.

3.4. Piecewise linear droop control

Alternatively, as proposed in [17] and also studied in [34], a combination of different droop gains can be used, resulting in a piecewise linear droop characteristic (Fig. 1d). Similar to the implementation with a droop control combined with a deadband or a constant voltage control, this control allows to distinguish between normal and disturbed operation. In this case, the voltage control law can be rewritten as

$$\chi = \chi_0 - \frac{1}{k_{dc}}(U_{dc} - U'_{dc,0}) - \frac{1}{k_{dc,0}}(U'_{dc,0} - U_{dc,0}), \tag{49}$$

with $k_{dc,0}$ the droop coefficient around the setpoint and k_{dc} a more stringent droop coefficient outside of this region (Fig. 1d). Similar equations can be written down for the power-and current-based droop.

3.4.1. Dynamic representation

In case of a power-based piecewise linear droop, ΔP_s is given by

$$\Delta P_s = \frac{1}{k_{dc}}(U_{dc} - U'_{dc,0}) + \frac{1}{k_{dc,0}}(U'_{dc,0} - U_{dc,0}), \tag{50}$$

which can directly be integrated with the control structure from Fig. 3.

In case of a current-based piecewise-linear droop control, ΔP_{dc} from (15) is reformulated as

$$\Delta P_{dc} = \Delta P_{dc_\gamma} + \Delta P_{dc_\delta}, \tag{51}$$

with the two contributing terms ΔP_{dc_γ} and ΔP_{dc_δ} now given by

$$\Delta P_{dc_\gamma} = -\frac{p}{k_{dc}}\left[\left(U_{dc}^2 - U_{dc,0}'^2\right) - U'_{dc,I0}\left(U_{dc} - U'_{dc,0}\right)\right] - \frac{p}{k_{dc,0}}\Delta U_{dc,0} \cdot |U_{dc} - U'_{dc,0}|, \tag{52}$$

$$\Delta P_{dc_\delta} = -\frac{p}{k_{dc,0}}\left[\left(U_{dc,0}'^2 - U_{dc,0}^2\right) - U'''_{dc,I0}\left(U'_{dc,0} - U_{dc,0}\right)\right], \tag{53}$$

with $U'_{dc,0}$ and $U'_{dc,I0}$ as respectively defined in (27) and (32) and $U'''_{dc,I0}$ as

$$U'''_{dc,I0} = U_{dc,0} + k_{dc,0} I_{dc,0}. \tag{54}$$

Fig. 4b shows these two contributions. The expression for ΔP_{dc_γ} largely coincides with that of ΔP_{dc_α} and accounts for the outer droop characteristic. The second term in the expression takes into account the setpoint shift by the inner droop characteristic, causing a minor contribution outside of the deadband. The expression for ΔP_{dc_δ} accounts for the inner droop characteristics and is constant outside of the deadband. Is is clear from Fig. 4 that the inner droop characteristic, which is mainly represented by ΔP_{dc_δ}, has an opposite effect in terms of the power contribution compared to a deadband (represented by ΔP_{dc_β} in Fig. 4a).

3.4.2. Steady-state representation

Since the piecewise-linear droop characteristic can be considered as the combination of two droop characteristics, the power flow equations become

$$P_{dc,0_i}^{(j)} = P_{dc_i}(\boldsymbol{U_{dc}}^{(j)}) + \frac{1}{k_{dc_i}}(U_{dc_i}^{(j)} - U'_{dc,0_i}) + \frac{1}{k_{dc,0_i}}(U'_{dc,0_i} - U_{dc,0_i}), \tag{55}$$

with $U'_{dc,0_i}$ at bus i as defined in (27). The change in the droop characteristic leads to a redefinition of the Jacobian elements. Expression (19) remains valid, whereas and (20) changes to

$$\left(U_{dc_i}\frac{\partial P_{dc,0_i}}{\partial U_{dc_i}}\right)^{(j)} = \left(U_{dc_i}\frac{\partial P_{dc_i}}{\partial U_{dc_i}}\right)^{(j)} + \alpha_i'^{(j)}, \tag{56}$$

with now

$$\alpha_i'^{(j)} = \begin{cases} k_{dc,0_i}^{-1} U_{dc,i}^{(j)} & \text{if } U_{dc_i}^{(j)} = U'_{dc,0_i} \\ k_{dc_i}^{-1} U_{dc,i}^{(j)} & \text{if } U_{dc_i}^{(j)} \neq U'_{dc,0_i} \end{cases}. \tag{57}$$

In case of a current-based droop characteristic the non-diagonal Jacobian elements (24) remain the same and (25) is redefined as

$$\left(U_{dc_i}\frac{\partial I_{dc,0_i}}{\partial U_{dc_i}}\right)^{(j)} = U_{dc_i}^{(j)} \sum_{\substack{j=1 \\ j\neq i}}^{n} Y_{dc_{ij}} + \alpha_i'^{(j)}. \tag{58}$$

with $\alpha_i'^{(j)}$ from (57).

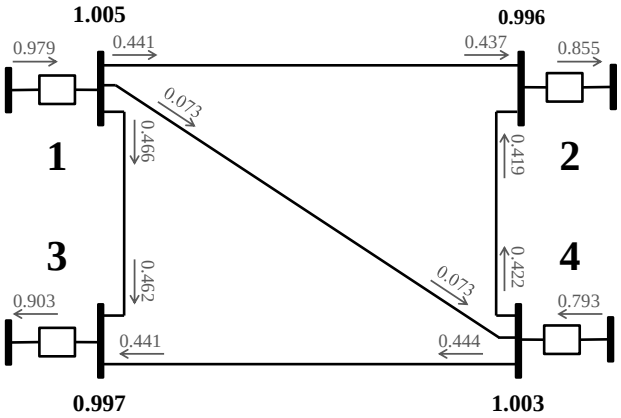

Figure 6: Initial conditions of the test system

4. Simulation results

4.1. Test system

In this section, simulation results are discussed for the different droop control strategies, implemented in a 4-terminal meshed HVDC grid of which the initial status is shown in Fig. 6. The power flow results,

encompassing both the initial results and the steady-state results after an outage, have been obtained using MatACDC, an open-source Matlab-based ac/dc power flow program [35]. The source code has been modified to include all the different steady-state droop implementations discussed in this paper. The dynamic results have been obtained using MatDyn, an open-source Matlab-based transient stability program [36] using average converter models. The droop control has been added as external control loops, the inner loops are implemented using the cascaded control structure from [31], which has been altered for the inclusion of the constant voltage band according to Fig. 5. The dc lines have been implemented using π-equivalent circuits consisting of the dc line capacitances, resistances and inductances. A modified Euler ODE solver was used with a step size of 2e-4 s.

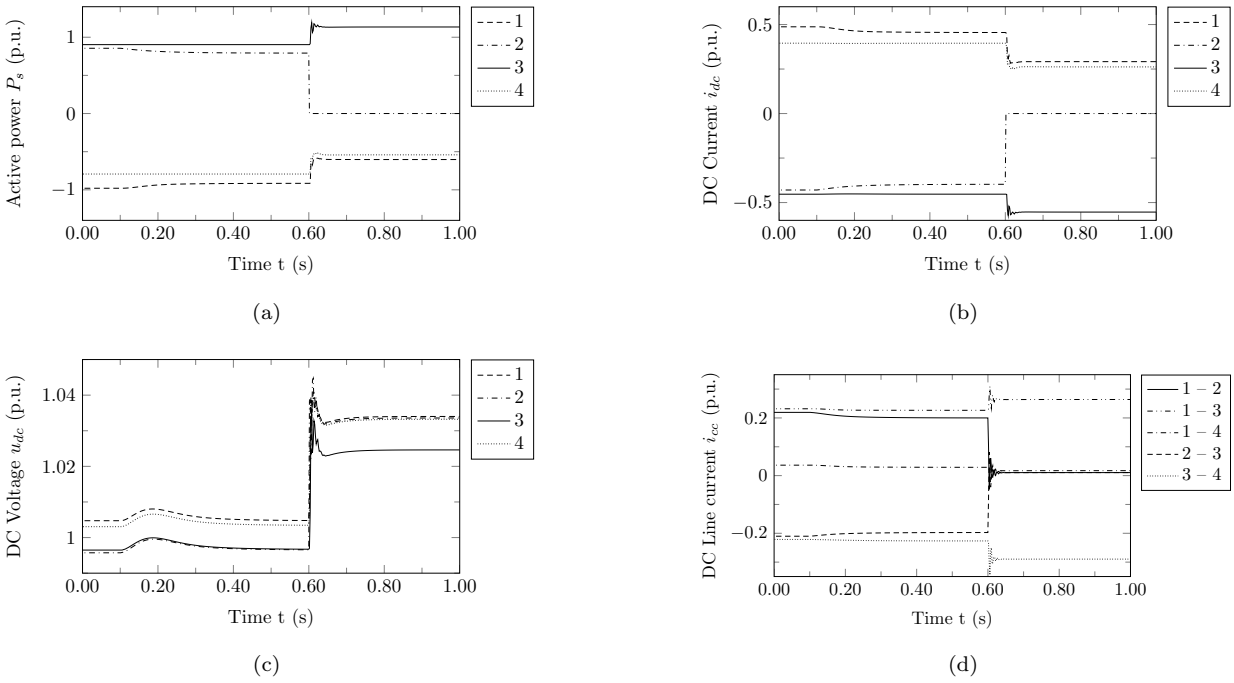

Figure 7: Setpoint change and outage of converter 2 : (a) Active power P_s injected into the ac grid , (b) dc-side currents i_{dc}, (c) dc-side voltage u_{dc} and (d) dc-side line currents i_{cc} .

4.2. Converter setpoint change and outage

Converter 1 from Fig. 6 is equipped with a power-based droop with a constant voltage band (Fig. 1c) with $\Delta P_{dc,0} = 0.083$ p.u. Converters 2 – 4 use a power-based droop controller with a constant power deadband (Fig. 1b) with $\Delta U_{dc,0} = 0.005$ p.u. Fig. 7 shows the results. At t = 0.1 s, the setpoint of converter 2 is slowly changed to 0.79 p.u. Converters 3 and 4 remain in constant power mode while converter 1 (constant voltage mode) takes the entire power imbalance. The dc-side current changes as a result of the change in system voltage. If a current-based droop control were implemented, the dc-side current would remain

constant and the active power would follow the change in system voltage. At t = 0.6 s, converter 2 faces an outage, which causes all converters to change their power according to the droop characteristics. The droop constant k_{dc} has been chosen equal to 10% for all converters.

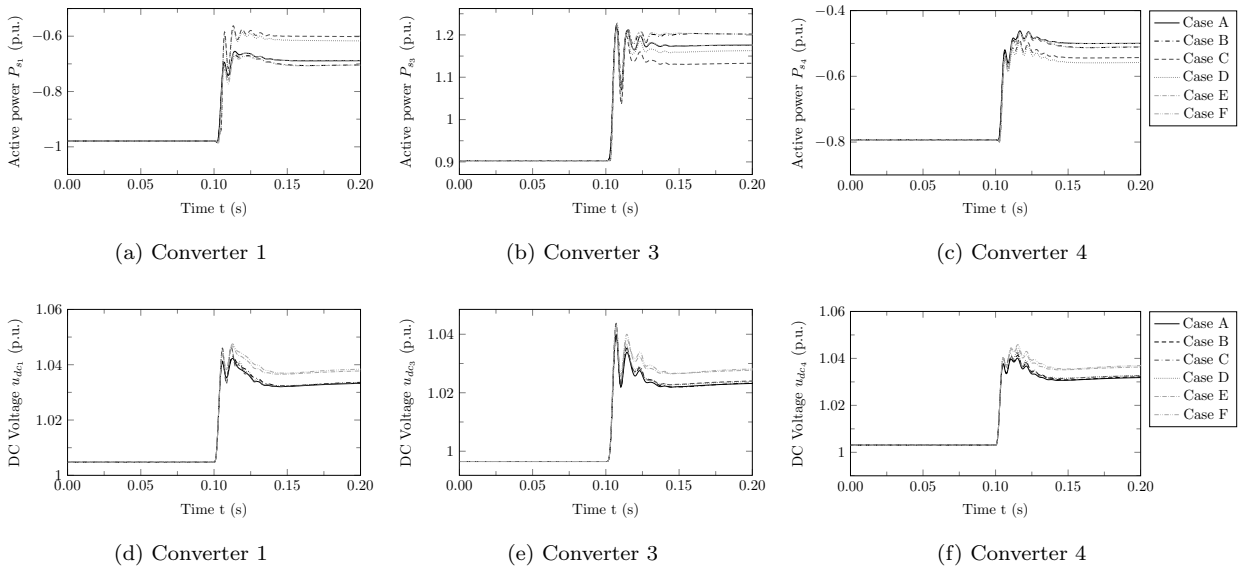

(a) Converter 1 (b) Converter 3 (c) Converter 4

(d) Converter 1 (e) Converter 3 (f) Converter 4

Figure 8: System response at converters 1 and 4 following an outage of converter 2 for different control modes. Active power P_s: converter 1 (a), 3 (b) and 4 (c) and dc-side voltage u_{dc}: converter 1 (d), 3 (e) and 4 (f) . **Legend:** Case A: P-droop, B: I-droop, C: P-droop with deadband (Converter 1: $\Delta P_{dc,0}$ and 2 – 4: $\Delta U_{dc,0}$), D: I-droop with deadband (Converter 1: $\Delta I_{dc,0}$ and 2 – 4: $\Delta U_{dc,0}$), E: P-droop, piecewise-linear, F: I-droop, piecewise-linear.

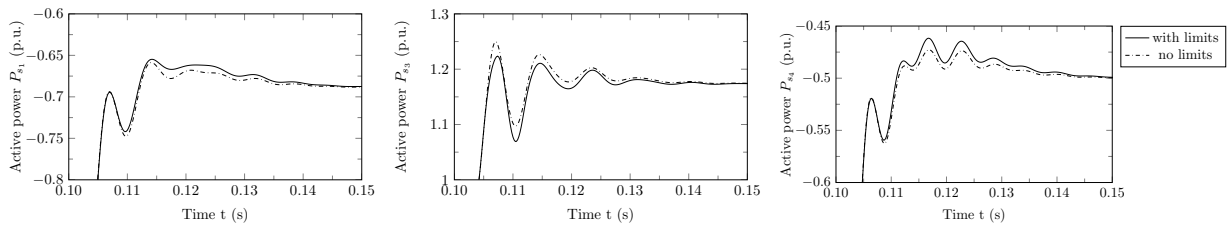

(a) Converter 1 (b) Converter 3 (c) Converter 4

Figure 9: Effect of dynamic current limiting in converter 3 on the dynamic power sharing (Case A: standard droop control).

4.3. Control mode comparison

Fig. 8 shows the response of converters 1, 3 and 4 for an outage of converter 2 at t = 0.1 s. Six different cases combining eight different control implementations are considered: the first two cases A and B consider respectively power- and current-based droop control without a deadband (Fig. 1a). Cases C and D consider droop control with a constant power/current deadband (Fig. 1b) for converters 2 – 4 and a droop control

with a constant voltage band (Fig. 1c) for converter 1. Cases E and F consider a piecewise linear droop characteristic (Fig. 1d) on all converters, respectively power- and current-based. The current-based droop k_{dc} has been chosen equal to 20 %, thus double that of the power-based droop constant, corresponding the definition from (12). In case of a piecewise linear droop, $k_{dc,0}$ has been chosen equal to $10 \cdot k_{dc}$, thus resulting in a steeper slope around the reference point.

It can be observed from the simulation results that the differences between the power-based droop control (cases A, C and E) and the current-based droop control (cases B, D and F) mainly are reflected in the steady-state values after the power flow, due the change in the dc-side voltages. The difference in dynamic response for the power-and current-based counterparts (respectively cases A & B, C & D and E & F) is relatively small. This leads to the conclusion that when a similar underlying control structure is used, the dynamic responses for different droop characteristics can be expected to be similar. It can also be observed that the constant power/current deadband in cases C and D does not lead to a higher dc-side voltage due to the fact that converter 1 takes a larger share of the power, thereby preventing the dc-side voltage from rising further, which is what would have been expected intuitively as a result of the inclusion of a deadband in converters 2 to 4. In case E and F, on the contrary, the inclusion of a steeper droop characteristic around the reference point for all converters does result in a larger dc-side voltage rise. In cases B and F, the power at converter 3 is limited to the maximum value, which is implemented as a limit to the current reference value i^*_{cq} (as e.g. in Fig. 5). In all other cases, the inner converter current reference limit in converter 3 is hit as well, but only during the transient phase. Fig. 9 shows the effect of this control limit, which causes a temporary limitation of the inner converter current reference at 1,2 p.u. Since the unbounded response is not much larger than the one where the limit is hit (Fig. 9b), the overall effect on the system dynamics and other converter powers is relatively small (Figs. 9a & 9c).

From the detailed results in Fig. 10, it is clear that including a constant voltage band in converter 1 (cases C and D) results in a larger initial response by this converter, and eventually, a higher share of the power distribution compared to the other cases (Fig. 10a). The opposite reasoning holds for converter 4, where the deadband delays the initial response, resulting in slightly lower initial power oscillations compared to the other cases (Fig. 10c). The difference between a power- and a current based droop control is not pronounced in the initial dynamic response of either control implementation and is mainly resulting in different steady-state values. The piecewise linear control with relaxed control settings around the reference setpoint (case E and F) results in a less stringent initial control action, allowing for slightly more pronounced initial voltage oscillations after the contingency at converter 1 (Fig. 10d) and to a lesser extent at converters 3 & 4 (Figs. 10e & 10f). The effect of the dynamic current reference limit in converter 3 is clear from the fact that all powers are approximately equal at the peak of the first swing (Fig. 10b). Table 1 shows the corresponding steady-state operating points after the contingencies as calculated by the power flow algorithm MatACDC. The difference between the power flow calculations and the steady-state values of the dynamic simulations

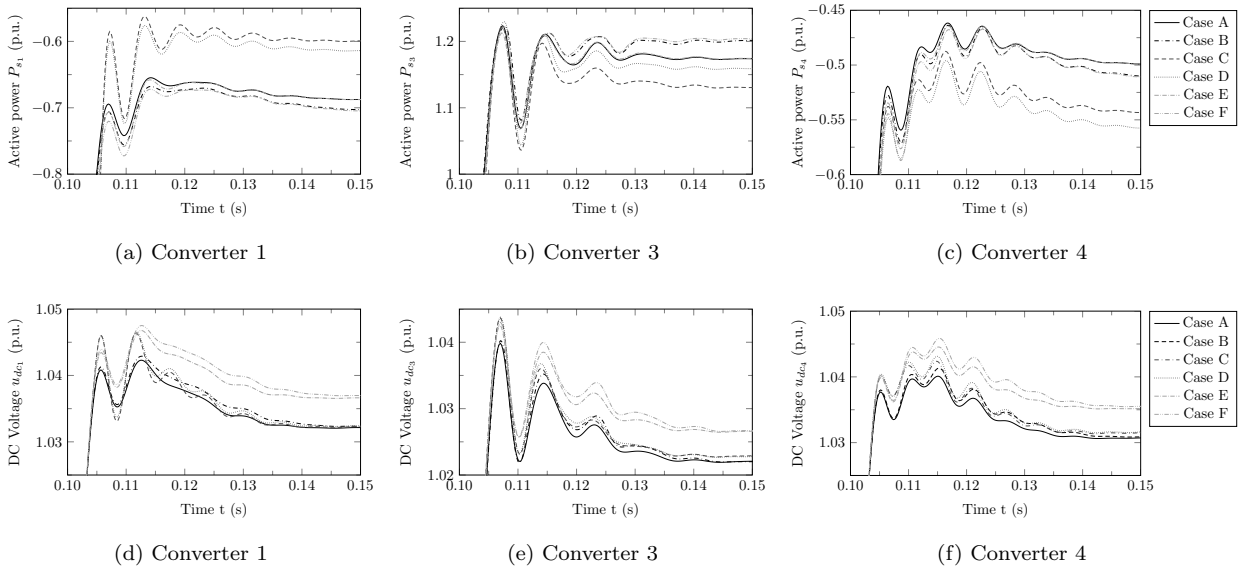

(a) Converter 1 (b) Converter 3 (c) Converter 4

(d) Converter 1 (e) Converter 3 (f) Converter 4

Figure 10: Detailed system response at converters 1, 3 and 4 following an outage of converter 2 for different control modes. **Legend:** See Fig. 8

(after t = 2.0 s) show almost exact correspondence: the differences are in the order of magnitude of the stop criteria of the algorithms. A larger difference could be expected when converter losses would be added to the steady-state power flow, since it would be difficult to account for their changes in the dynamic analysis as a result of the changing operating conditions. In cases B and F, the current limit in converter 3 is also hit at the end of the simulation, which is adequately modeled in the steady-state analysis as well by including the converter operation limits to the power flow algorithm, turning the droop controlled bus to a constant power representation as soon as operation outside of the limits is detected. The results confirm the observation from Fig. 10, namely that the piecewise droop characteristics (cases E & F) yield almost similar results in terms of power injections when compared to the standard droop control (cases A & B), whereas the steady-state voltages are higher as a result of inclusion of a the steeper droop characteristic around the reference point.

Table 1: Converter powers and voltages after the outage of converter 2 (power flow results)

	$P_{s_1}(p.u.)$	$U_{dc_1}(p.u.)$	$U_{dc_2}(p.u.)$	$P_{s_3}(p.u.)$	$U_{dc_3}(p.u.)$	$P_{s_4}(p.u.)$	$U_{dc_4}(p.u.)$
case A: P-droop	-0.6878	1.0339	1.0331	1.1760	1.0238	-0.4991	1.0324
case B: I-droop	-0.7023	1.0343	1.0335	1.2000	1.0240	-0.5090	1.0328
case C: P-droop, $\Delta P_{dc,0}$	-0.6030	1.0340	1.0336	1.1343	1.0246	-0.5413	1.0332
case D: I-droop, $\Delta I_{dc,0}$	-0.6183	1.0341	1.0337	1.1638	1.0245	-0.5560	1.0333
case E: P-droop, $k_{dc,0}$	-0.6880	1.0384	1.0376	1.1763	1.0283	-0.4992	1.0369
case F: I-droop, $k_{dc,0}$	-0.7027	1.0391	1.0383	1.2000	1.0288	-0.5085	1.0376

5. Conclusion

In this paper, the different droop control strategies available in the literature have been analytically derived, implemented and compared. The main contribution of this paper lies in the development of a comprehensive modeling framework for the different droop-based control schemes available in literature. All different droop control models have been implemented in both a steady-state power flow algorithm and a dynamic simulation program. Simulation results show a good correspondence between the implementations in both types of programs. It is shown that when the various controls are implemented using a comparable underlying control structure, the different converter droop characteristics give rise to a similar dynamic response after a contingency. Hence, little differences are perceived between power- and current-based droop control in terms of dynamic response. By comparing the dynamic responses with the post-fault steady-state results obtained using a power flow analysis for different droop characteristics, it can be concluded that the power flow analysis allows an accurate prediction of the steady-state power flow and voltage changes after all the different control actions. Therefore, the need for time-consuming dynamic simulations to determine the post-contingency system operation can be eliminated if the dynamic control response is not of interest.

Acknowledgement

The research of Jef Beerten is funded by a research grant from the Research Foundation – Flanders (FWO).

References

[1] D. Van Hertem, M. Ghandhari, Multi-terminal VSC HVDC for the European supergrid: Obstacles, Renewable and Sustainable Energy Reviews 14 (9) (2010) 3156–3163. doi:DOI: 10.1016/j.rser.2010.07.068.

[2] R. Hendriks, G. Paap, W. Kling, Control of a multi-terminal VSC transmission scheme for connecting offshore wind farms, in: Proc. European Wind Energy Conference & Exhibition, Milan, Italy, 2007, 8 pages.

[3] T. Haileselassie, K. Uhlen, T. Undeland, Control of multiterminal HVDC transmission for offshore wind energy, in: Proc. Nordic Wind Power Conference Presentation, Rønne, Denmark, 2009, 7 pages.

[4] T. Nakajima, S. Irokawa, A control system for HVDC transmission by voltage sourced converters, in: IEEE PES Summer Meeting, 1999, Vol. 2, 1999, pp. 1113–1119.

[5] W. Lu, B.-T. Ooi, DC overvoltage control during loss of converter in multiterminal voltage-source converter-based HVDC (M-VSC-HVDC), IEEE Trans. Power Del. 18 (3) (2003) 915–920. doi:10.1109/TPWRD.2003.813888.

[6] T. M. Haileselassie, M. Molinas, T. Undeland, Multi-terminal VSC-HVDC system for integration of offshore wind farms and green electrification of platforms in the North Sea, in: Proc. NORPIE 2008, Espoo, Finland, 2008, 8 pages.

[7] T. K. Vrana, J. Beerten, R. Belmans, O. B. Fosso, A classification of DC node voltage control methods for HVDC grids, Electric Power System Research. 103 (2013) 137 – 144.

[8] C. Dierckxsens, K. Srivastava, M. Reza, S. Cole, J. Beerten, R. Belmans, A distributed DC voltage control method for VSC MTDC systems, Electric Power Systems Research 82 (1) (2012) 54–58.

[9] J. Beerten, R. Belmans, Modeling and control of multi-terminal VSC HVDC systems, Energy Procedia 24 (2012) 123–130, selected papers from Deep Sea Offshore Wind R&D Conference, Trondheim, Norway, Jan. 19–20, 2012.

[10] T. M. Haileselassie, K. Uhlen, Impact of DC line voltage drops on power flow of MTDC using droop control, IEEE Transactions on Power Systems 27 (3) (2012) 1441–1449.

[11] P. Rault, Dynamic modeling and control of multi-terminal HVDC grids, Ph.D. thesis, Ecole Centrale de Lille (Mar. 2014).

[12] E. Prieto-Araujo, F. D. Bianchi, A. Junyent-Ferre, O. Gomis-Bellmunt, Methodology for droop control dynamic analysis of multiterminal VSC-HVDC grids for offshore wind farms, IEEE Transactions on Power Delivery 26 (4) (2011) 2476–2485. doi:10.1109/TPWRD.2011.2144625.

[13] O. Gomis-Bellmunt, J. Liang, J. Ekanayake, N. Jenkins, Voltage-current characteristics of multiterminal HVDC-VSC for offshore wind farms, Electric Power Systems Research 81 (2011) 440–450.

[14] W. Wang, M. Barnes, O. Marjanovic, Droop control modelling and analysis of multi-terminal VSC-HVDC for offshore wind farms, in: Proc. IET ACDC 2012, Birmingham, UK, 2012, 6 pages.

[15] C. Barker, R. Whitehouse, Autonomous converter control in a multi-terminal HVDC system, in: Proc. IET ACDC 2010, London, UK, 2010, 5 pages.

[16] CIGRÉ Working Group B4-52, HVDC grid feasibility study, Final report (Apr. 2013).

[17] T. K. Vrana, L. Zeni, O. B. Fosso, Active power control with undead-band voltage & frequency droop for HVDC converters in large meshed DC grids, in: EWEA 2012 - European Wind Energy Conference & Exhibition, Copenhagen, Denmark, 2012, pp. 612–616.

[18] A. Egea-Alvarez, J. Beerten, D. V. Hertem, O. Gomis-Bellmunt, Hierarchical power control of multiterminal HVDC grids, Electric Power Systems Research 121 (2015) 207 – 215. doi:http://dx.doi.org/10.1016/j.epsr.2014.12.014.

[19] R. Eriksson, A new control structure for multi-terminal dc grids to damp inter-area oscillations, IEEE Transactions on Power Delivery, 8 pages, accepted for publication. doi:10.1109/TPWRD.2014.2364738.

[20] R. Preece, J. Milanovic, Tuning of a damping controller for multiterminal VSC-HVDC grids using the probabilistic collocation method, IEEE Transactions on Power Delivery 29 (1) (2014) 318–326. doi:10.1109/TPWRD.2013.2258945.

[21] J. Beerten, R. Belmans, Analysis of power sharing and voltage deviations in droop-controlled DC grids, IEEE Transactions on Power Systems 28 (4) (2013) 4588–4597. doi:10.1109/TPWRS.2013.2272494.

[22] X. Zhao, K. Li, Droop setting design for multi-terminalHVDC grids considering voltage deviation impacts, Electric Power Systems Research 123 (2015) 67 – 75. doi:http://dx.doi.org/10.1016/j.epsr.2015.01.022.

[23] J. Dragon, L. Werner, J. Hanson, Effects of DC voltage droop characteristics on contingency behaviour of AC/DC systems, in: In Proc. International Universities' Power Engineering Conference (UPEC) 2014, Cluj-Napoca, Romania, 2014, 6 pages. doi:10.1109/UPEC.2014.6934686.

[24] S. Akkari, M. Petit, J. Dai, X. Guillaud, Interaction between the voltage-droop and the frequency-droop control for multi-terminal HVDC systems, in: Proc. IET ACDC 2015, Brimingham, UK, 2015, , 7 pages.

[25] I. Martinez Sanz, B. Chaudhuri, G. Strbac, Inertial response from offshore wind farms connected through DC grids, IEEE Transactions on Power Systems 30 (3) (2015) 1518–1527. doi:10.1109/TPWRS.2014.2349739.

[26] M. Aragüés-Peñalba, A. Egea-Àlvarez, O. Gomis-Bellmunt, A. Sumper, Optimum voltage control for loss minimization in HVDC multi-terminal transmission systems for large offshore wind farms, Electric Power Systems Research 89 (2012) 54–63. doi:10.1016/j.epsr.2012.02.006.

[27] L. Zhang, Modeling and control of VSC-HVDC links connected to weak AC systems, Ph.D. thesis, Royal Institute of Technology, (KTH), Stockholm, Sweden (2010).

[28] N. R. Chaudhuri, B. Chaudhuri, Adaptive droop control for effective power sharing in multi-terminal DC (MTDC) grids, IEEE Transactions on Power Systems 28 (1) (2013) 21–29. doi:10.1109/TPWRS.2012.2203390.

[29] B. Berggren, K. Linden, R. Majumder, DC grid control through the pilot voltage droop concept – methodology for

establishing droop constants, IEEE Transactions on Power Systems, 9 pages, accepted for publication.

[30] W. Wang, A. Beddard, M. Barnes, O. Marjanovic, Analysis of active power control for VSC-HVDC, IEEE Transactions on Power Delivery 29 (4) (2014) 1978–1988. doi:10.1109/TPWRD.2014.2322498.

[31] J. Beerten, S. Cole, R. Belmans, Modeling of multi-terminal VSC HVDC systems with distributed DC voltage control, IEEE Transactions on Power Systems 29 (1) (2014) 34 – 42.

[32] D. Jovcic, A. J. Far, A three level cascaded VSC controller and testest on CIGRE B4.58 DC grid test system, in: Proc. CIGRÉ Belgium Conference, Brussels, Belgium, 2014, 8 pages.

[33] J. Beerten, D. Van Hertem, R. Belmans, VSC MTDC systems with a distributed DC voltage control – a power flow approach, in: Proc. IEEE PowerTech '11, Trondheim, Norway, 2011, 6 pages. doi:10.1109/PTC.2011.6019434.

[34] C. Barker, R. Whitehouse, Further developments in autonomous converter control in a multi-terminal HVDC system, in: Proc. IET ACDC 2012, Birmingham, UK, 2012, 6 pages.

[35] MatACDC website.
URL `http://www.esat.kuleuven.be/electa/teaching/matacdc/`

[36] S. Cole, R. Belmans, MatDyn, a new Matlab-based toolbox for power system dynamic simulation, IEEE Transactions on Power Systems 26 (3) (2011) 1129–1136.